Role of Hydrogen Bonding Interactions in Directing One-Dimensional Thiol-Assisted Growth of Silver-Based Nanofibers

Emil Avier Hernandez, Bertina Posada, Roberto Irizarry,† and Miguel E. Castro*

Chemical Imaging Center, Department of Chemistry, The University of Puerto Rico at Mayaguez, Mayaguez, Puerto Rico 00680

Received: December 17, 2004; In Final Form: February 14, 2005

We present evidence, based on scanning and transmission electron microscopy measurements, for the formation of nanofibers from silver−thiol materials treated with water. Mercapto acetic acid, a thiol with a carboxylic acid group at one end, was employed for the experiments presented here. Nanoparticles, with diameters as large as 1 nm, fill the nanofibers and are responsible for absorption bands between 2 and 5.5 eV in UV−visible absorption spectroscopy measurements. The nanofibers disappear at pH values larger than the first pK_a of the acid, while rods are observed for pH values between 3.6 and 7. This result is interpreted in the context of hydrogen bonding interactions playing an important role in driving the one-dimensional growth of the fibers, a proposal that is supported by the vibrational frequency of the carbonyl stretching mode in surface reflection Fourier transform infrared measurements on dry deposits of aqueous dispersions of the thiol−silver material.

1. Introduction

There is considerable interest in the synthesis of nanostructures that exhibit a larger degree of structural complexity than particles, including nanowires, nanorods, nanofibers, and nanotubes. Many efforts are focused on the synthesis and characterization of nanostructures of noble metals, such as silver, due to the ease of characterization employing standard techniques, particularly optical absorption spectroscopy.[1−10] Synthesis of silver nanowires and rods, for instance, has received significant attention in recent years due to the broad impact they may have in future scientific and technological developments. Large aspect ratio nanowires can be important components of nanoscale circuits requiring long electrical connections.[1−5] Short aspect ratio nanowires and rods, on the other hand, are suitable for the fabrication of antennas for wireless and remote communication applications and substrates for surface-enhanced Raman scattering (SERS) measurements.[7−10] Nanotubes and nanofibers may find applications as devices to store high-energy chemicals and drugs. Meshlike arrangements of these nanostructures may also find applications in engineering membranes and use as components for the remediation of damaged neural systems. Methods based in wet chemistry for large-scale production of these nanostructres are, with little doubt, an important step in the commercialization of nanoscale electronics and future scientific breakthroughs.

We report in this paper on a wet chemical approach to the synthesis of nanofibers based on silver−thiol materials prepared from the reaction of mercaptoacetic acid and silver nitrate. In contrast to previous works related to the synthesis of nanostructures, the approach presented here does not rely on templates to form the nanofibers. The nanofibers are observed at pH values smaller than the pK_a of the thiol that corresponds to the equilibrium for the conversion of the thiol carboxylic acid functionality into a carboxylate anion, while smaller linear formations survive to pH values slightly larger than 7.0. This result is interpreted in terms of a thiol mediated assembly mechanism that involves hydrogen bonding interactions among the carboxylic acid groups of the thiol to drive the one-dimensional growth of the nanofibers. Surface reflection Fourier transform spectroscopy (FTIR) is very sensitive to the presence of carboxylate anions and hydrogen bonded carboxylic acid groups, and measurements on dry deposits of aqueous dispersions of the thiol−silver material that lead to the nanofibers in the carbonyl stretching frequency are consistent with this proposal. Scanning and transmission electron microscopies reveal that the nanofibers are filled with nanoparticles with diameters as large as 1 nm. UV−visible absorption measurements are consistent with the presence of such silver nanoparticles as well as with smaller silver nanoclusters.

2. Experimental Section

Silver nitrate and mercaptoacetic acid were obtained from Kodak and Aldrich, respectively, and used without further purification. HPLC-quality water was employed in all dilutions reported here. Unless otherwise specified, samples were allowed to dry in the dark for 24−48 h prior to electron microscopy or vibrational spectroscopy measurements.

An environmental JEOL 6460 HV/LV scanning electron microscope and a JEOL 1200 FX transmission electron microscope were employed for the imaging measurements reported here. Scanning electron microscopy (SEM) images were acquired with a secondary electron detector coupled to a PC. Transmission electron microscopy (TEM) images were acquired with a standard film and developed in a darkroom using routine procedures. A 14 nm gold colloid was employed as a calibration standard in the TEM measurements. A Matheson Fourier transform infrared spectrometer coupled to an Olympus microscope equipped with a aluminum-coated Cassegrain objective with a magnification factor of 15 was employed for the

* To whom correspondence should be addressed. E-mail: mcastro@uprm.edu.

† Permanent address: Dupont Microelectronics, Manati, Puerto Rico 00680.

10.1021/jp044242n CCC: $30.25
Published on Web 03/19/2005

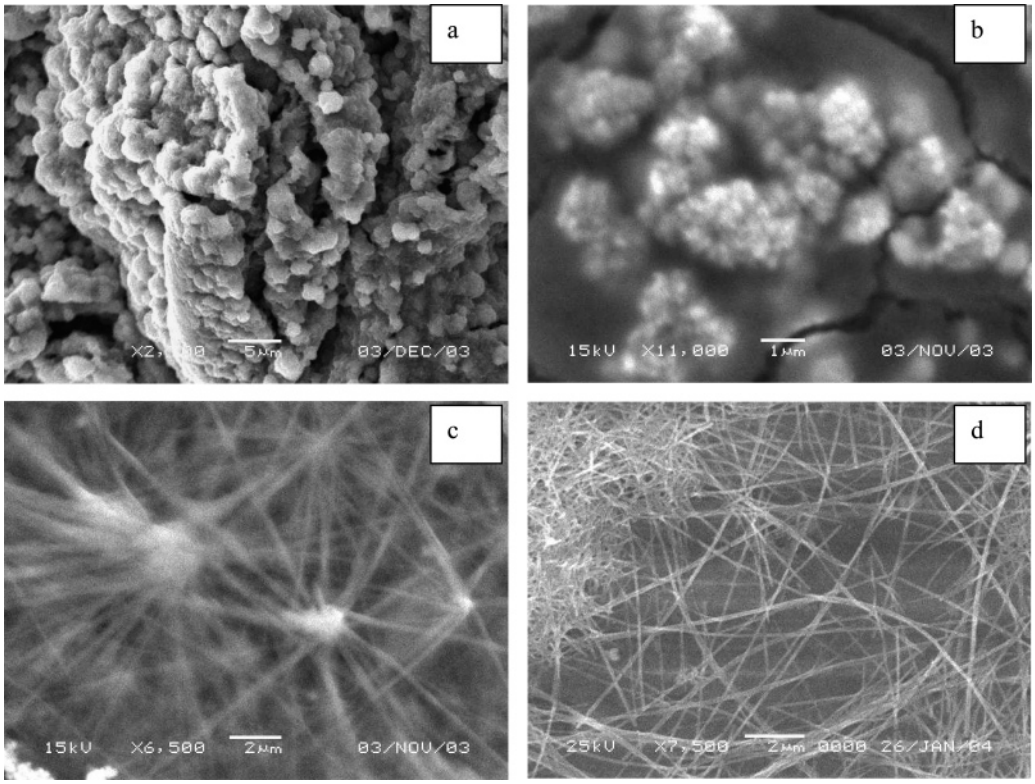

Figure 1. SEM images of dry deposits of silver−thiol material treated with (a) 0, (b) 0.010, (c) 0.5, and (d) 10 mL of water. The thiol to silver molar ratio is 1.3 in all samples.

vibrational spectroscopy work. Unless otherwise specified, all FTIR spectrosopy measurements reported here were performed in the surface reflection mode. The X-ray photoemission measurements were performed in a PHI 5600 system equipped with an optical microscope that allowed pinpointing the location of the deposits to be examined on the substrate surface. UV−visible absorption spectroscopy measurements were performed with a computer-integrated Ocean Optics UV PC 2000 spectrometer and a deuterium lamp and a standard CUV-FL-DA cuvette holder. A high transmission fiber optic was employed to interface the light transmitted through the sample compartment into the spectrometer.

3. Results and Discussion

3.1. Thiol−Silver Material Synthesis. A yellow solid is formed upon the addition of mercaptoacetic acid to solid $AgNO_3$. The color of the material changes to red a few seconds after the formation of the material. The addition of water causes marked changes in the morphology of the yellow material. SEM images and corresponding surface reflection FTIR spectra in the carbonyl stretching region (between 1500 and 1800 cm^{-1}) of dry deposits of the thiol−silver material as a function of the amount of water added are displayed in Figures 1 and 2, respectively. The as-prepared material consists predominantly of large particle agglomerates. The corresponding surface reflection FTIR spectrum is consistent with the presence of carboxylate anions in the material, as judged by the broad band between 1550 and 1650 cm^{-1}, which is typically found in carboxylate anions.[12−16] The addition of 10 μL of water segregates the material into agglomerates of the particles. Bands due to carboxylate anions (1590 cm^{-1}) and carboxylic acids (1702 cm^{-1}) are identified in the carbonyl stretching region of the corresponding surface reflection FTIR spectrum. Fibers of various diameters and lengths emerge from the particle agglomerates in dry deposits of silver−thiol materials treated with 500 μL of water. A band centered at 1710 cm^{-1} due to the neutral form of the carboxylic acid dominates the carbonyl stretching region of the surface reflection FTIR spectrum. A dispersion of white flakes is formed upon the addition of 10 mL of water to the yellow material. SEM images of dry deposits

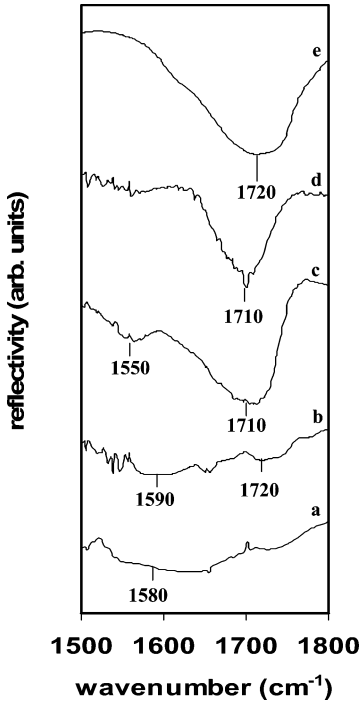

Figure 2. Surface reflection FTIR spectra of dry deposits of a silver−thiol material treated with (a) 0, (b) 0.010, (c) 0.5, and (d) 10 mL of water. The thiol to silver molar ratio is 1.3 in all samples. The transmission FTIR spectrum of a liquid sample of thiol is labeled (e) in the figure.

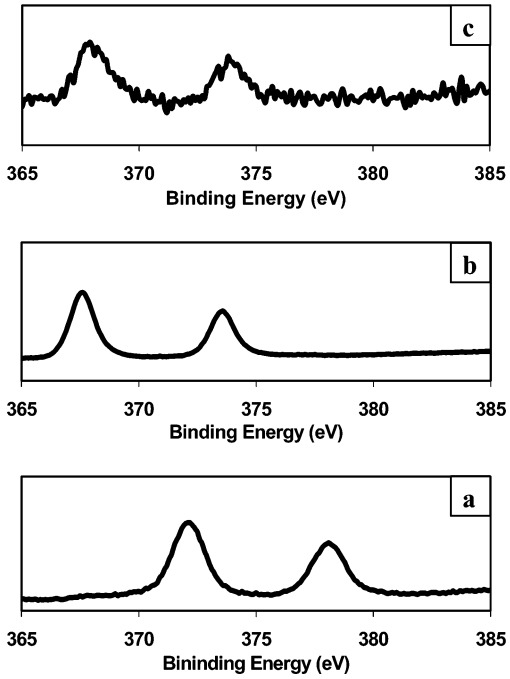

Figure 3. Ag $3d_{5/2}$ and Ag $3d_{3/2}$ photoemission spectra of (a) solid $AgNO_3$, (b) silver reference standard, and (c) a 5 μL deposit prepared with a thiol to $AgNO_3$ ratio of 1.3 and diluted with 10.0 mL of water.

of the dispersions reveal the formation of nanofibers of various lengths and diameters: not a single particle is observed in SEM images of over 50 samples of the thiol−silver material treated with this large amount of water. Deposits allowed to dry for over 48 h are composed of fibers similar to those illustrated in the image displayed in Figure 1d, indicating that the material in the dry deposit is converted into nanofibers. Thus the fibers are the principal product of the process described above. Furthermore, these formations are observed on a number of substrates where the deposits were allowed to dry for the SEM measurements, including plastics and metal oxides, indicating that the formation of the nanofibers is substrate independent, and that the formations are driven by strong attractive interactions among the constituents of the deposit. The carbonyl stretching frequency in the corresponding surface reflection FTIR spectrum is centered at 1710 cm^{-1}, about 10 and 90 cm^{-1} lower than the value found for pure thiol in the liquid and gas phases, respectively. The lowering of the carbonyl stretching frequency in carboxylic acids is typically discussed in the context of strong hydrogen bonding interactions.[28] In the gas phase, the average intermolecular distance is large enough to prevent such interactions.[28] In the liquid, however, hydrogen bonding interactions have the effect of lowering the carbonyl stretching frequency.[28] The value found for the carbonyl stretching frequency in dry deposits of the thiol−silver material is consistent with the existence of hydrogen bonding interactions in the dry deposits studied here.

3.2. X-ray Photoemission Measurements. X-ray photoemission spectroscopy (XPS) measurements were performed on dry deposits of the aqueous dispersions with the purpose of establishing the chemical state of silver in the white flakes. The results are summarized in Figure 3. Metallic silver exhibits peaks at 367.4 and 373.4 eV due to photoelectron emission from the Ag $3d_{5/2}$ and Ag $3d_{3/2}$ bands, respectively, while the bands are about 1 eV higher in the XPS spectrum of Ag_2O reported in the literature.[14,15] These bands appear at 371.8 and 377.8 eV in the XPS spectrum of silver in solid $AgNO_3$. The Ag $3d_{5/2}$ and Ag $3d_{3/2}$ peaks are centered at 367.6 and 373.7 eV, respectively, in the XPS of deposits formed from dispersions prepared by diluting a mixture of $AgNO_3$ and thiol with 10 mL of water. The position of the Ag $3d_{3/2}$ and Ag $3d_{5/2}$ photoemission peaks is, within the uncertainty of the measurements, consistent with the presence of reduced silver in deposits formed from dispersions prepared by diluting the thiol−silver material with 10 mL of water. The bands are slightly broader than corresponding bands in the silver reference, with a full peak width at half the peak maximum of 1.63 eV, as well as being asymmetric, tailing toward slightly higher binding energies, indicating that more than one type of silver is present in the deposits. Within the sensitivity of the instrument employed for the measurements, bands that could be attributed to Ag^+ cations in the XPS spectrum of dry deposits formed from dispersions prepared by diluting the thiol−silver material with 10 mL of water are not observed, indicating that no silver cations are present in the deposits.

The reactions that result in the reduction of silver cations by mercaptoacetic acid are not established in this work. Sulfhydryl groups are known to add to silver in many cases; for instance, cysteine, a sulfur-containing amino acid, is known to react with silver cations by the sulfur end of the molecule.[36] It is very likely that under the conditions of our experiments these thiolates are oxidized to organic sulfur oxides ($R-SO_x$), which are known to form upon air exposure of alkanethiol monolayers on silver.[29,30] An extensive amount of sulfur is present in our XPS chamber and prevents a straightforward interpretation of sulfur XPS bands and binding energies in our samples. Further speculation is unwarranted until a systematic work is performed to establish the reduction mechanism of silver in the presence of mercaptoacetic acid.

3.3. UV−Visible Absorption Spectroscopy. UV−visible absorption measurements of aqueous dispersions with several thiol to $AgNO_3$ mole ratios are also consistent with the reduction of silver cations. The absorption spectra of two aqueous dispersions of silver and thiol mixtures are displayed in Figure 4. For reference, the dashed lines in Figure 4 indicate the absorption spectra of corresponding amounts of thiol diluted in water. The thiol absorbs strongly between 5 and 4.5 eV, with a tail that extends to 4 eV: the positions of these bands were found to be insensitive to solution pH.

The UV−visible absorption spectra of aqueous dispersions of the material with a thiol to silver ratio of 0.4 exhibit a broad absorption band between 5 and 3.3 eV with a low-energy tail that extends to 1.5 eV. Well-defined peaks at 4.8 and 4.7 eV, a shoulder at about 4.4 eV, a broad band between 3.4 and 3.7 eV, and a low-energy shoulder at about 2.7 eV are observed in the absorption spectrum upon increasing the thiol to silver ratio to 1.3. Light absorption in this region is well-known to result from excitations in several forms of silver, including Ag^0 (3.9−4.2 eV) and charged (Ag_2^+, Ag_4^{2+}) and uncharged silver clusters.[19−22] The XPS measurements discussed in the previous paragraphs allow us to rule out the presence of charged silver clusters, such as Ag_2^+ or Ag_4^{2+}. O'Shea and co-workers have measured the $3d_{3/2}$ and $3d_{5/2}$ binding energies of silver cluster ions.[31] Binding energies for the 3d XPS peaks of these silver cluster ions are about 3 eV higher than corresponding silver bands in diluted thiol−silver materials.

Fedrigo et al. have examined the photoabsorption spectra of silver clusters containing from 2 to 21 atoms.[23] Clusters containing between 2 and 21 silver atoms exhibit a number of bands between 2.5 and 4.5 eV. The cluster that contains two silver atoms (Ag_2) is the only one with well-resolved peaks around 4.7 and 4.8 eV, in close similarity to the spectra of

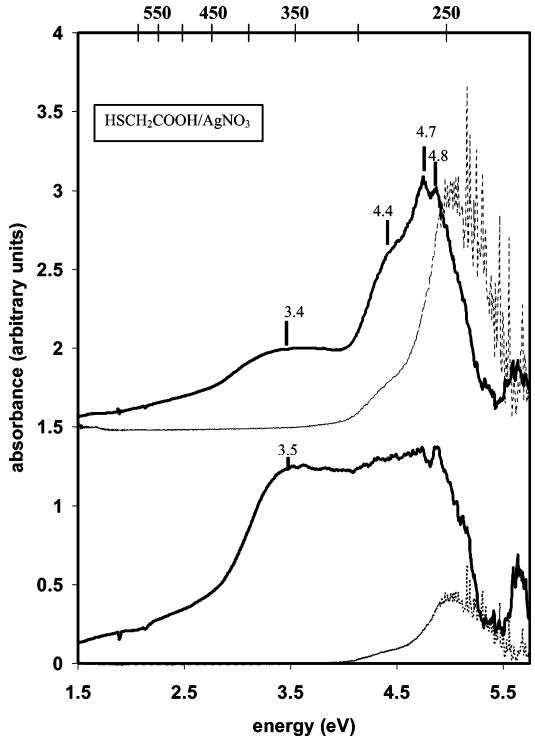

Figure 4. UV−visible absorption spectra of aqueous dispersions with a thiol to silver ratio of 1.3 (upper trace) and 0.4 (lower trace). Aqueous silver nitrate was employed as a reference for the measurements. The absorption spectra of the corresponding amounts of thiol are indicated by the dashed lines in the figure. The upper horizontal scale corresponds to the absorption wavelengths in nm.

aqueous dispersions of thiol−silver materials displayed on Figure 4. The Ag_2 cluster, as well as clusters with up to 11 atoms, also exhibits low-energy bands between 2.8 and 3.2 eV, which does not allow us to assign the absorption spectra displayed in Figure 4 to Ag_2 exclusively. The optical absorption spectra of clusters containing more than 11 silver atoms, on the other hand, are dominated by a band between 3 and 4 eV.[19−23] This band is also observed in the spectra of aqueous dispersions of the thiol−silver material. The multiple absorption features observed in the spectra of aqueous dispersions of silver and thiol mixtures lead us to conclude that polydisperse silver particles, with at least two different sizes, are present in the dispersions. The reader should keep in mind that these particles are present in a dispersion containing mercaptoacaetic acid. Thus the particle surfaces are likely covered by thiol or thiolate molecules, as discussed in the previous section.

3.4. Electron Microscopy Measurements. A typical transmission electron microscopy image of dry deposits of a mixture of $AgNO_3$ and thiol diluted with 10.0 mL of water is displayed in Figure 5. The dispersion was shaked vigorously and a standard 3 mm copper grid was immersed in the solution for a few seconds and allowed to dry in air for 5 min before it was placed in the TEM sample compartment. Islands of dense deposits were typically found in TEM images of deposits prepared using the method described above. The primary beam energy of the TEM employed for the measurements reported here allowed us to obtain clear images of the edge of the deposits. The nanofibers identified in SEM measurements in previous paragraphs are readily identified in the TEM image. TEM allows imaging these nanostructures in greater detail than SEM measurements. The nanostructures are between 15 and 30 nm in diameter, while their length varies from about 230 nm to several micrometers.

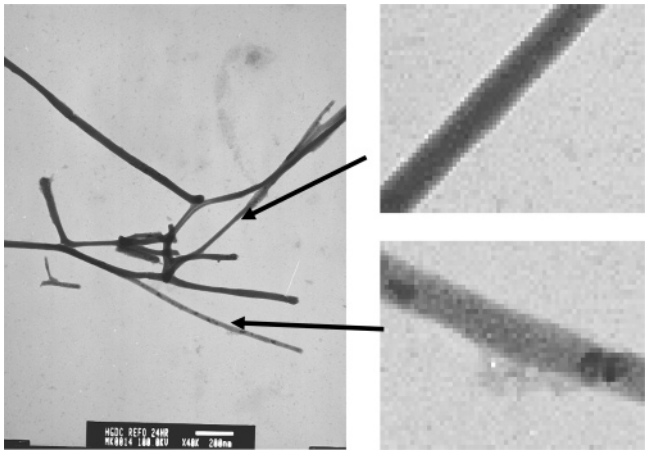

Figure 5. Electron microscopy images of dry deposits of a silver−thiol mixture diluted with 10.0 mL of water. The insets correspond to the regions indicated by the arrows magnified by a factor of ×500. The thiol to silver molar ratio is 1.3.

It is interesting that not a single "free" particle is observed in TEM images of dry deposits of aqueous dispersions of thiol−silver mixtures, despite the fact that their existence is suggested in the UV−visible absorption measurements. The particles, if present, must be inside the nanofibers. Inspection of the regions indicated by the arrows at higher magnifications confirms the presence of small particles inside the fibers. We were able to observe these formations in all the nanofibers examined in the TEM. The size of the particles is very difficult to determine from the images. We estimate an upper limit of 1 nm for the diameter of the particles that can be distinguished in the image. This particle size is considerably smaller than those reported in the literature for silver nanoparticle synthesis in basic media. Smaller structures, spaced by little more than 2 nm, were observed on the edges of the walls of the nanofibers, but the images are not resolved well enough to interpret them in terms of the silver dimer, Ag_2.

Electron diffraction measurements of the structures found inside the nanofibers displayed in the TEM image, as well as independent X-ray powder diffraction measurements on thicker samples, failed to show evidence for a diffraction pattern, a result that is consistent with noncrystalline particles in the nanofibers. The lattice constant of silver in a face-centered cube (fcc) is 0.409 nm.[32] We estimate that 1 nm particles are composed of about 40 atoms, if the atoms pack closely in an fcc crystal structure. This number of atoms may be too small to have a well-defined fcc unit cell. A number of structures and isomers for particles composed of small silver clusters, containing up to 21 atoms leading to particle sizes up to 0.8 nm, are predicted by theoretical calculations.[33,34] Even on silver nanoparticles with diameters as large as 3 nm the existence of faults and distortions is documented.[35] A close-packed fcc 3 nm sphere, however, contains over 1000 silver atoms. Thus the existence of noncrystalline silver in particles with diameters of 1 nm is not surprising.

3.5. pH-Dependent SEM and Surface Reflection FTIR Measurements. Scanning electron microscopy measurements were performed on dry deposits of aqueous dispersions of the thiol−silver material as a function of pH. SEM allows us to image regions that are not easily imaged with TEM due to the thickness of the deposits. The pH of a dispersion prepared by diluting the thiol−silver material with 10 mL of water is 2.9. The pH of the dispersion was determined with a commercial pH meter calibrated with standard buffer solutions. Dispersions with a lower or larger pH value were prepared by the addition

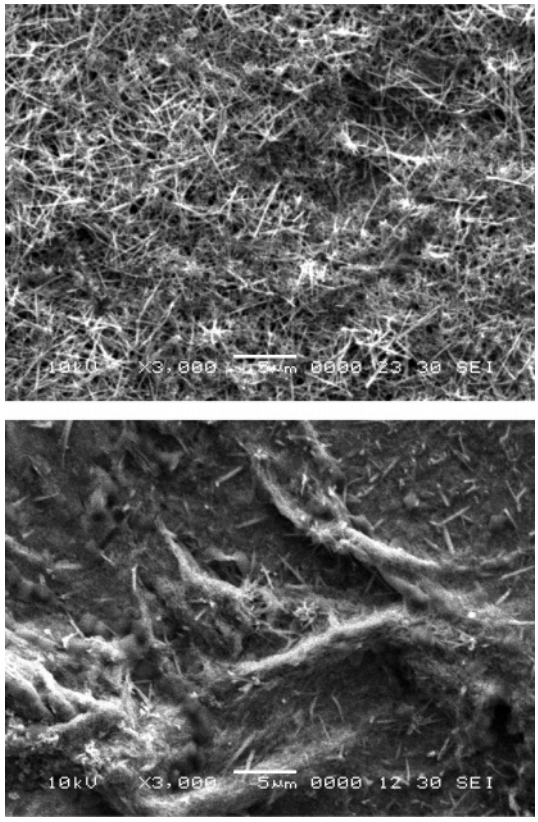

Figure 6. SEM images of dry deposits of aqueous dispersions of $AgNO_3$ and thiol reaction mixtures prepared at (upper) pH 0.9 and (lower) pH 6.2.

of 10 mL of acidic or basic water, respectively. Acidic and basic water were prepared with stock solutions of nitric acid (HNO_3) or sodium hydroxide (NaOH). Representative SEM images of dry dispersions at a pH 0.9 and pH 6.2 are displayed in the upper and lower panels of Figure 6, respectively. At pH 0.9, the nanofibers dominate the SEM image, while rods are the only nanostructure observed in SEM images of dry deposits of dispersions prepared at the higher pH. The rods have an average length of (2.3 ± 0.5) μm.

The density of nanostructures, defined as the number of fibers or rods per square micrometer (μm^2), is displayed in Figure 7. The density of nanostructures was estimated from SEM measurements performed on 5 μL deposits of dispersions prepared as described in the previous paragraph. The nanostructure density decreases with the pH of the dispersion until it reaches a pH value of 7.5; no nanostructures are observed at and above this pH. In passing, we note that not a single particle is observed in SEM measurements of dry deposits of the thiol−silver material diluted with 10 mL of water, although they are the only structures observed when the thiol−silver material is treated with 10 μL of water.

Mercaptoacetic acid has two acidic protons, one associated with the carboxylic acid functionality and the other bonded to the sulfur atom. The pK_a values of the first and second equilibria are 3.6 and 10.5, which correspond to formation of the carboxylate anion and the loss of the hydrogen bonded to the sulfur atom to form a thiolate, respectively.[24] The splitting of nanofibers and rods above and below the pH values that correspond to the first pK_a of mercaptoacetic acid is consistent with a proposal that hydrogen bonding interactions among carboxylic acid groups play an important role in the formation of the nanofibers observed in the TEM and SEM images. At pH values of 0.9 and 2.9, for instance, we estimate the ratio of

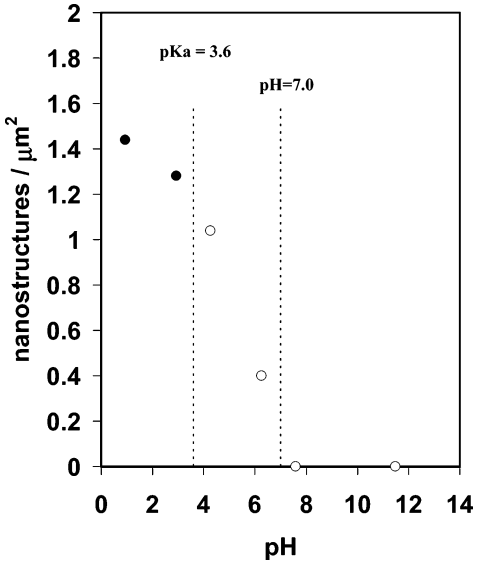

Figure 7. Density of nanostructures per μm^2 as a function of pH. The filled and open circles indicate the number of nanofibers and rods, respectively, per μm^2.

carboxylic acid concentrations to be about 0.82, in close agreement with the ratio of the corresponding density of nanofibers, which is estimated to be 0.89. Therefore, as the carboxylic acid concentration decreases with pH, the number of fibers observed in the corresponding SEM images decreases.

Hydrogen bonding interactions have been proposed to play a significant role in directing the alignment of one-dimensional mixed copper and silver metal polymer chains of Ag[Cu(2-methylpyrazine-5-carboxylate)$_2$·$(H_2O)_2$](BF_4) and Ag[Cu(2-methylpyrazine-5-carboxylate)$_2$·$(H_2O)_2$](NO_3).[25,37−39] The vibrational frequency of the carbonyl group, determined from Fourier transform infrared spectroscopy−attenuated total reflection measurements (FTIR−ATR), has been used to establish the role of hydrogen bonding interactions in directing the layer-by-layer growth of mononuclear films of polyacids from aqueous solution.[26] Multilayers of polyacid films were found to disintegrate gradually with increasing pH value, with a sharp dropoff in the multilayer concentration around pH 7. The vibrational frequency of the carbonyl was found to decrease with pH due to formation of the carboxylate anion forms of the acids, which in turn represents a reduction in the number of COOH groups available for hydrogen bonding.[26]

Surface reflection FTIR spectroscopy measurements on dry deposits of aqueous dispersions of thiol−silver mixtures prepared at pH 2.9 and 4.3 are displayed in Figure 8. The carbonyl stretching frequency is centered at 1705 cm^{-1} in the vibrational spectrum of deposits prepared by diluting the thiol−silver mixture with water at pH 2.9. The strong hydrogen bonding interactions in the mixture shifts this frequency down by 85 cm^{-1} as compared to the value found in the gas phase for mercaptoacetic acid.[27,28] The intensity of the 1705 cm^{-1} band is drastically reduced in the vibrational spectrum of dry deposits of the thiol−silver material diluted with 10 mL of water at pH 4.3. The spectrum is dominated by a broad and asymmetric band centered at 1640 cm^{-1} typically associated with the carbonyl stretching mode in carboxylate anions.[12−16,26] This result is consistent with our interpretation that hydrogen bonding interactions play an important role in the formation of the nanofibers observed in the TEM and SEM images presented in Figures 1 and 5.

The formation of carboxylic acid dimers through hydrogen bonding interactions is well documented.[25,28] In aqueous solu-

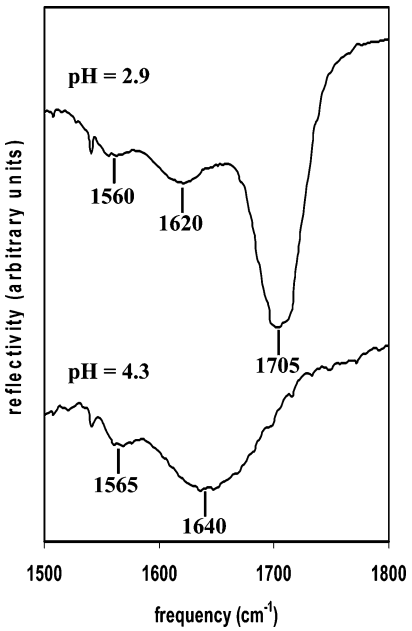

Figure 8. Surface reflection FTIR measurements of dry deposits of aqueous dispersions of thiol−silver material diluted with 10 mL of water and at pH 2.9 (upper trace) and pH 4.3 (lower trace). The thiol to silver ratio in the mixture is 1.3.

tion, carboxylic acids form hydrogen bonds largely with water molecules. In the aqueous dispersions reported here, the ratio of water molecules to carboxylic acid groups is nearly 5×10^4 to 1. Thus most of the carboxylic acid groups are solvated by water molecules in the aqueous dispersions. Upon removal of water, as in dry deposits of the material, hydrogen bonding interactions among carboxylic acid groups takes place, as evidenced in the surface reflection FTIR measurements discussed in the previous paragraphs. These interactions are strong enough to drive the one-dimensional growth of the nanofibers observed in the TEM and SEM images reported here. We were not able to pinpoint a pH or a chemical combination of reactants that could result in the synthesis of monodisperse nanofibers. Work in progress in this laboratory using negatively charged anions has had limited success in the control of the aspect ratio of the nanofibers.

Recent works in other groups have taken advantage of hydrogen bonding interactions to introduce longitudinal or three-dimensional order at the nanoscale.[37−39] Thioalkanecarboxylic acids are reported to play a central role in the longitudinal alignment of gold nanorods.[37] Carboxylic acid capped gold nanoparticles self-assemble to form two- or three-dimensional superlattices.[38] The work presented here adds nicely to these previous works and supports the hypothesis that hydrogen bonding interactions, such as those present among carboxylic acid groups, may find technological applications in driving order in nanostructures.

4. Summary

In summary, we have presented evidence in this paper for the reduction of silver in the presence of mercaptoacetic acid to form structures dominated by particle agglomerates. The addition of water to the material results in changes in the morphology of the nanostructures. Nanofibers, which are filled with particles, are observed in dry deposits of aqueous dispersions of the thiol−silver material. Formation of the nanofibers is insensitive to the nature of the substrate used to dry the deposits. The nanofibers are observed at pH values lower than the first pK_a of mercaptoacetic acid, while rods are the dominant nanostructures for pH values between the first pK_a and pH 7.5. These nanostructures are no longer observed for pH values above 7.5. Hydrogen bonding interactions are proposed to play a central role in directing the formation of nanofibers.

Acknowledgment. Financial support from the National Science Foundation, Nanotechnology Undergraduate Education Program (Award No. 0304348) is gratefully acknowledged. M.E.C. wishes to thank Dr. David Harling, manager of The JEOL Institute, and Dr. Jonathan King, from the Biology Department of the Massachusetts Institute of Technology, for their assistance with the TEM measurements. The authors wish to thank Dr. Luis Sola, from Dupont Microelectronics, for helpful discussions and for the XRD measurements. Financial support from the Puerto Rico LSAMP undergraduate research program and the Sloan Undergraduate Research Program (2000-5-22-AP) is gratefully acknowledged. M.E.C. dedicates this work to the memory of G.E.P.

References and Notes

(1) Bhattacharrya, S.; Saha, S. K.; Chakravorty, D. *Appl. Phys. Lett.* **2000**, *76*, 3896.
(2) Bhattacharrya, S.; Saha, S. K.; Chakravorty, D. *Appl. Phys. Lett.* **2000**, *77*, 3770.
(3) Sauer, G.; Brehm, G.; Schneider, S.; Nielsch, K.; Wehrspohn, R. B.; Choi, J.; Hofmeister, H.; Gosele, U. *J. Appl. Phys.* **2002**, *91*, 3243.
(4) Barbic, M.; Mock, J. J.; Smith, D. R.; Shultz, S. *J. Appl. Phys.* **2002**, *91*, 9341.
(5) Chang, J.; Chang, J.; Lo, B.; Tzing, S.; Ling, Y. *Chem. Phys. Lett.* **2003**, *379*, 261−267.
(6) Tan, Y.; Jiang, L.; Li, Y.; Zhu, D. *J. Phys. Chem. B* **2002**, *106*, 3131−3138.
(7) Tao, A.; Kim, F.; Hess, C.; Goldberg, J.; He, R.; Sun, Y.; Xia, Y.; Yang, P. *Nano Lett.* **2003**, *3*, 1229−1233.
(8) Jana, N. R.; Gearheart, L.; Murphy, C. J. *Chem. Commun.* **2001**, 617−618.
(9) Michaels, A. M.; Jiang, J.; Bruss, L. *J. Phys. Chem. B* **2000**, *104*, 11965−11971.
(10) Moskovits, M. *Rev. Mod. Phys. I* **1985**, *57*, 783−826.
(11) Wei, G.; Nan, C.; Deng, Y.; Lin, Y. *Chem. Mater.* **2003**, *15*, 4436−4441.
(12) Lee, J. Y.; Painter, P. C.; Coleman, M. M. *Macromolecules* **1988**, *21*, 346.
(13) Lu, X.; Weiss, R. A. *Macromolecules* **1995**, *28*, 3022.
(14) Dong, J.; Ozaki, Y.; Nakashima, K. *Macromolecules* **1997**, *30*, 1111.
(15) Painter, P. C.; Pehlert, G. J.; Hu, Y. H.; Coleman, M. M. *Macromolecules* **1999**, *32*, 2055.
(16) Ataka, K.; Hegemann, P.; Heberle, J. *Biophys. J.* **2003**, *84*, 466−474.
(17) Moulder, J. F.; Stickle, W. F.; Sobol, P. E.; Bomben, K. D. *Handbook of X-ray Photoelectron Spectroscopy*; Physical Electronics Inc: Eden Praire, MN, 1995.
(18) Cai, W.; Tan, M.; Wang, G.; Zhang, L. *Appl. Phys. Lett.* **1996**, *69*, 2980−2982.
(19) Dimitrijevic, N. M.; Bartels, D. M.; Jonah, C. D.; Takahashi, K.; Rajh, T. *J. Phys. Chem. B* **2001**, *105*, 954−959.
(20) Andrews, M. P.; Ozin, G. A. *J. Phys. Chem.* **1986**, *90*, 2929−2938.
(21) ten Kortenaar, M. V.; Kolar, Z. I.; Tichelaar, F. D. *J. Phys. Chem. B* **1999**, *103*, 2054−2060.
(22) Lin, X. Z.; Teng, X.; Yang, H. *Langmuir* **2003**, *19*, 10081−10085.
(23) Fedrigo, S.; Harbich, W.; Buttet, J. *Phys. Rev. B* **1993**, *47*, 10706−10715.
(24) Harris, D. C. *Quantitative Chemical Analysis*; Freeman and Co.: New York, NY, 2003.
(25) Dong, Y.; Smith, M. D.; zur Loye, H. *Inorg. Chem.* **2000**, *39*, 1943−1949.
(26) Sukhishvili, S. A.; Granick, S. *Macromolecules* **2002**, *35*, 301−310.
(27) Mallard, W. G. *National Institute of Standards and Technology Chemistry Web Book*; National Institute of Standards and Technology: Washington, DC, 2003.
(28) Vinogradov, S. N.; Linnell, R. H. *Hydrogen Bonding*; Van Nostrand Reinhold Company: New York, NY, 1971.

(29) Schoenfisch, M. H.; Pemberton, J. E. *J. Am. Chem. Soc.* **1998**, *120*, 4502−4513.
(30) Tarlov, M. J.; Newman, J. G. *Langmuir* **1992**, *8*, 1398−1405.
(31) O'Shea, J. N.; Schnadt, J.; Andersson, S.; Patthey, L.; Rost, S.; Giertz, A.; Brena, B.; Forsell, J.; Sandell, A.; Bjorneholm, O.; Bruhwiler, P. A.; Martensson, N. *J. Chem. Phys.* **2000**, *113*, 9233−9238.
(32) Smith, W. F. *Foundations of Materials Science and Engineering*; McGraw-Hill, Inc.: New York, 1993.
(33) Zhao, J.; Luo, Y.; Wang, G. *Eur. Phys. J.* **2001**, *14*, 309−316.
(34) Bonačić-Koutecky, V.; Veyret, V.; Mitrić, R. *J. Chem. Phys.* **2001**, *115*, 10450−10460.
(35) Nepijko, S. A.; Levlev, D. N.; Shulze, W.; Urban, J.; Ertl, G. *Chem. Phys. Chem.* **2000**, *3*, 140−142.
(36) Rensing, C.; Ghosh, M.; Rosen, B. P. *J. Bacteriol.* **1999**, *181*, 5891−5897.
(37) Thomas, K. G.; Barazzouk, S.; Ipe, B. I.; Joseph, S. T. S.; Kamat, P. V. *J. Phys. Chem. B* **2004**, *108* (35), 13066−13068.
(38) Yao, H.; Kojima, H.; Sato, S.; Kimura, K. *Langmuir* **2004**, *20* (23), 10317−10323.
(39) Zhang, X.; Zhao, Q.; Tian, Y.; Xie, Y. *Cryst. Growth Des.* **2004**, *4* (2), 355−359.